# Karyopherin α-3 is a key protein in the pathogenesis of spinocerebellar ataxia type 3 controlling the nuclear localization of ataxin-3

Anna Sergeevna Sowa[a,b,c], Elodie Martin[d], Inês Morgado Martins[a,b], Jana Schmidt[a,b], Reinhard Depping[e], Jonasz Jeremiasz Weber[a,b], Franziska Rother[f,g], Enno Hartmann[f], Michael Bader[f,g,h], Olaf Riess[a,b], Hervé Tricoire[d], and Thorsten Schmidt[a,b,1]

[a]Institute of Medical Genetics and Applied Genomics, University of Tuebingen, 72076 Tuebingen, Germany; [b]Center for Rare Diseases, University Hospital Tuebingen, 72076 Tuebingen, Germany; [c]Graduate School of Cellular and Molecular Neuroscience, University of Tuebingen, 72074 Tuebingen, Germany; [d]Degenerative Processes, Stress and Aging, CNRS UMR 8251, University Paris Diderot–Paris 7, 75205 Paris, France; [e]Institute of Physiology, University of Luebeck, 23538 Luebeck, Germany; [f]Institute of Biology, University of Luebeck, 23538 Luebeck, Germany; [g]Max-Delbrueck-Center for Molecular Medicine, 13125 Berlin, Germany; and [h]Charité-University Medicine Berlin, 10117 Berlin, Germany

Edited by Huda Y. Zoghbi, Baylor College of Medicine, Jan and Dan Duncan Neurological Research Institute at Texas Children's Hospital, Howard Hughes Medical Institute, Houston, TX, and approved January 4, 2018 (received for review October 9, 2017)

**Spinocerebellar ataxia type 3 (SCA3) is a neurodegenerative disorder caused by a CAG expansion in the *ATXN3* gene leading to a polyglutamine expansion in the ataxin-3 protein. The nuclear presence and aggregation of expanded ataxin-3 are critical steps in disease pathogenesis. To identify novel therapeutic targets, we investigated the nucleocytoplasmic transport system by screening a collection of importins and exportins that potentially modulate this nuclear localization. Using cell, *Drosophila*, and mouse models, we focused on three transport proteins, namely, CRM1, IPO13, KPNA3, and their respective *Drosophila* orthologs Emb, Cdm, and Kap-α3. While overexpression of CRM1/Emb demonstrated positive effects in *Drosophila*, KPNA3/Kap-α3 emerged as the most promising target, as knockdown via multiple RNAi lines demonstrated its ability to shuttle both truncated and full-length expanded ataxin-3, rescue neurodegeneration, restore photoreceptor formation, and reduce aggregation. Furthermore, *KPNA3* knockout in SCA3 mice resulted in an amelioration of molecular and behavioral disturbances such as total activity, anxiety, and gait. Since KPNA3 is known to function as an import protein and recognize nuclear localization signals (NLSs), this work unites ataxin-3 structure to the nuclear pore machinery and provides a link between karyopherins, NLS signals, and polyglutamine disease, as well as demonstrates that KPNA3 is a key player in the pathogenesis of SCA3.**

neurodegeneration | spinocerebellar ataxia | polyglutamine expansion | ataxin-3 | karyopherin

Spinocerebellar ataxia type 3 (SCA3), also known as Machado–Joseph disease (MJD), belongs to the group of neurodegenerative disorders characterized by a polyglutamine expansion in the expressed protein of the disease-associated gene (1). Within the general human population, the *ATXN3* gene carries between 12 and 43 CAG repeats which are not associated with a phenotype, while patients carry between 51 and 91 repeats on the affected allele (2). The expansion in the protein leads to cellular dysfunction characterized by protein cleavage, mitochondrial dysfunction, autophagic disturbances, and protein aggregation (3). Ultimately, this leads to the observed phenotype characterized by a disturbance of movement coordination (cerebellar ataxia); bulbar, pyramidal, and extrapyramidal signs; and a possible occurrence of peripheral neuropathy or ophthalmoplegia (4). Currently, there is no cure or therapy mitigating disease progression available for SCA3.

In the 20 y since the disease protein has been uncovered, protein aggregation has remained the hallmark feature of SCA3 and other polyglutamine disorders, including SCA1, 2, 7, 17, spinobulbar muscular atrophy, dentatorubral-pallidoluysian atrophy, and Huntington's disease (HD). Targeting and measuring aggregation remains the benchmark for disease progression and is assessed in recent studies dealing with drug efficacy and disease outcomes (5–7). The nuclear presence of aggregates is of unique importance, as nuclear expanded protein has been shown to have a direct correlation with toxicity (8–10). We have previously confirmed that, as long as full-length ataxin-3 (even with an extremely expanded polyglutamine stretch of 148Q) is in the cytoplasm, it remains harmless (10), while its localization to the nucleus is a key component of toxicity. In the process of clarifying the mechanisms controlling this intracellular localization of ataxin-3, we identified two nuclear export signals (NESs) and one weak nuclear localization signal (NLS) within the primary sequence of ataxin-3 (11). NLSs are known to be recognized by karyopherins, a group of proteins which belong to the machinery of the nuclear pore complex (NPC), which serves as the entry point for proteins into and out of the nucleus.

Karyopherins, also known as importins or exportins, act as receptors which bind cargo using various NES and NLS signals, translocate the cargo through the NPC, and release it on the other side (12). The signaling landscape surrounding transport proteins suggests a connection to neurodegeneration. For example, the whole nuclear transport machinery was affected in response to reactive oxygen species-mediated stress (13). Transport proteins

## Significance

**Ataxin-3 is the affected protein in the neurodegenerative disorder spinocerebellar ataxia type 3 (SCA3). Nuclear ataxin-3 has been linked to disease progression and formation of aggregates. Our present findings implicate karyopherin alpha 3 (KPNA3) in the in vitro transport of ataxin-3 and in the SCA3-related phenotypes in *Drosophila* and mouse models. We have demonstrated that altering transport proteins has an effect on both pathogenic mechanisms (e.g., the intracellular localization and the formation of aggregates) and key features of ataxin-3 toxicity such as anxiety, total activity, and gait abnormalities. A better appreciation of this cellular mechanism can enhance our understanding of polyglutamine diseases and the role of nuclear/cytoplasmic compartments in toxicity and clearance of ataxin-3.**

Author contributions: A.S.S., E.M., I.M.M., J.S., R.D., J.J.W., E.H., M.B., O.R., H.T., and T.S. designed research; A.S.S., E.M., I.M.M., J.S., R.D., J.J.W., F.R., H.T., and T.S. performed research; A.S.S., E.M., J.S., R.D., J.J.W., F.R., E.H., M.B., H.T., and T.S. contributed new reagents/analytic tools; A.S.S., E.M., J.S., R.D., H.T., and T.S. analyzed data; and A.S.S., E.M., J.S., R.D., O.R., H.T., and T.S. wrote the paper.

The authors declare no conflict of interest.

This article is a PNAS Direct Submission.



[1]To whom correspondence should be addressed. Email: thorsten.schmidt@med.uni-tuebingen.de.

This article contains supporting information online at www.pnas.org/lookup/suppl/doi:10.1073/pnas.1716071115/-/DCSupplemental.

Published online February 23, 2018.

are also intimately involved in the signaling pathways important to ataxin-3, such as activation of Erk, changes in transport of nuclear factor-κB (14), activating-transcription factor 2, and the transcription factor CREB (15, 16). The androgen receptor is dependent on karyopherins for nuclear import (17), and huntingtin possesses CRM1 export signals as well as karyopherins' β1/β2 (KPNB1/TNPO1) NLSs (18, 19). Transport proteins have also garnered attention in relation to amyotrophic lateral sclerosis (ALS) and frontotemporal lobar degeneration, where importins play a role in the observed nuclear protein depletion and cytoplasmic aggregation. This gave us evidence to postulate that transport proteins could also be involved in the nucleocytoplasmic trafficking and intracellular localization of ataxin-3, thereby influencing the toxicity and aggregation of ataxin-3 and, thus, the pathogenesis of SCA3.

We now report that KPNA3 (also known as importin alpha-4; GeneID 3839) is a key player in the intracellular localization of ataxin-3. We demonstrated in vitro and in vivo that KPNA3 controls the localization and aggregation of ataxin-3 as well as its toxicity. Down-regulation/knockout of *KPNA3* in *Drosophila* and mouse models alleviated the neurological phenotype induced by expanded ataxin-3. Our results provide support for the concept that transport proteins are involved in the disease progression of SCA3 and indicate KPNA3 as a highly promising therapeutic target for the treatment of SCA3.

## Results

**Nuclear Import of Ataxin-3 Is Mediated by the Classical Importin α/β Pathway via KPNA3 in HEK Cells.** Although ataxin-3 is predominantly localized in the cytoplasm of cells, it forms protein aggregates in the nucleus of neurons in SCA3 patients (20, 21). Since karyopherins are known to shuttle protein cargo across the nuclear/cytoplasmic membrane, we explored the role of these proteins in the nuclear transport of ataxin-3. Our previous analysis revealed a clear link between the intracellular localization of ataxin-3 and its propensity to aggregate (10). Therefore, using aggregation as a readout, we used FACS to isolate a population of cells equally expressing ataxin-3 148Q (stably transfected) and overexpressed transport proteins to analyze aggregate formation (Fig. 1*A*). Our screen of 12 transport proteins (Table S1) yielded KPNA3 and IPO13 as modulators of aggregation, as overexpression of the protein altered the total amount of aggregated ataxin-3 over a 96-h posttransfection window (Fig. 1*A* and Table S1). *CRM1* overexpression also showed an increase in aggregation which did not reach statistical

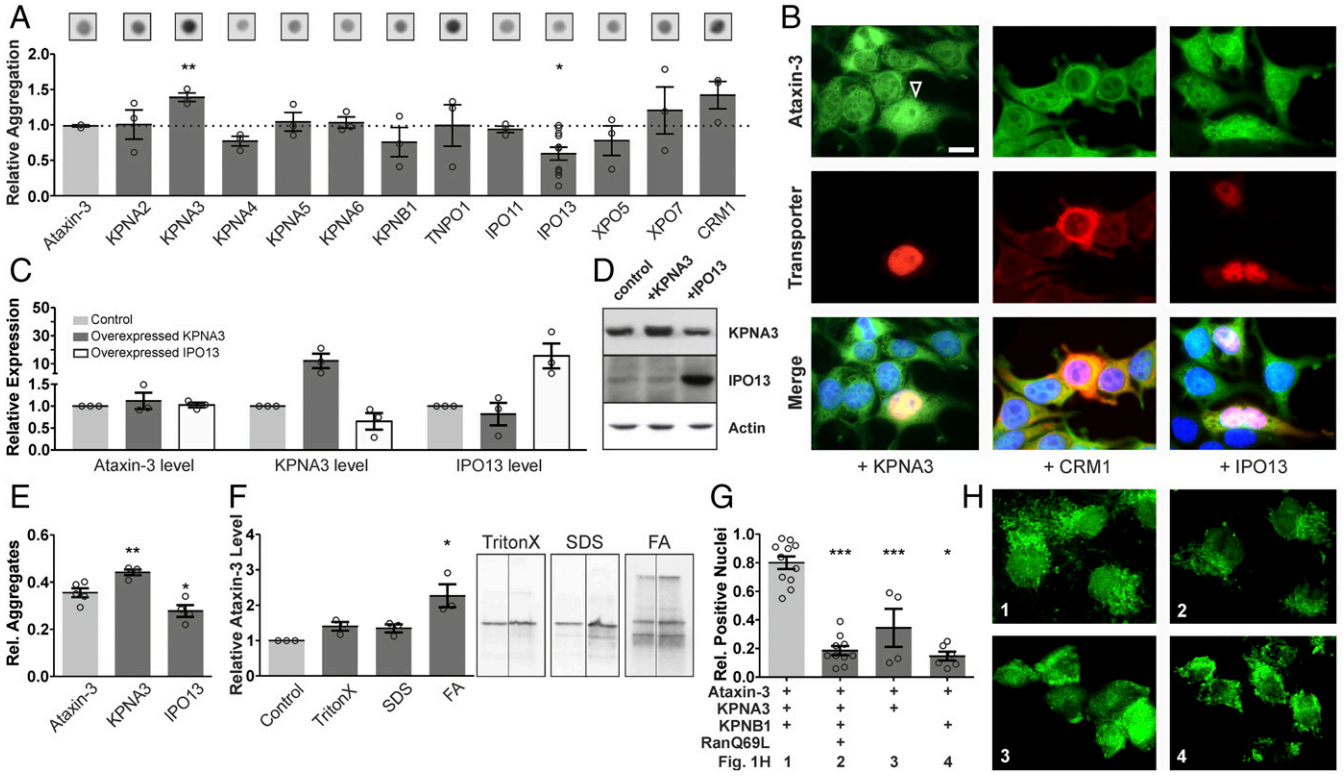


**Fig. 1.** Nuclear import of ataxin-3 is mediated by the classical importin α/β pathway via KPNA3. (*A*) Transport protein overexpression alters levels of aggregated expanded ataxin-3. *KPNA3* overexpression increases total aggregated ataxin-3 by filter trap. *IPO13* overexpression shows the strongest decrease. Representative filter trap dot images are shown from triplicates performed on the same filter. $n = 11$ for IPO13; $n = 3$ for all other measurements. Each experiment was conducted in triplicate and in dilutions. (*B*) Microscopy was used for a visual confirmation of altered localization. The cell coexpressing *KPNA3* (arrowhead) shows increased nuclear distribution of ataxin-3 compared with the neighboring cell without KPNA3. No significant changes were observed with CRM1 and IPO13. GFP signal is ataxin-3 148Q, red channel transport protein of interest. (Scale bar: 20 μm.) (*C* and *D*) Transport proteins were increased on a transcriptional and translational level: mRNA (*C*) and protein (*D*) in cells transfected with a cDNA control, *KPNA3*, or *IPO13* plasmid. Transcriptional levels of endogenous ataxin-3 are not altered upon transport protein overexpression. KPNA3 and IPO13 antibodies are per Table S2. (*E*) Total aggregation was verified by visual counting of HEK 293 cells transiently transfected with GFP-tagged ataxin-3. Ten fields were counted under blinded conditions. Number of cells with aggregates was calculated as percentage of total transfected cells. Values are displayed for $n = 6$. (*F*) Cell fractionation was performed according to Koch et al. (53). The formic acid (FA) faction shows a significant increase of insoluble aggregates of expanded ataxin-3 upon *KPNA3* overexpression. $n = 3$. Lanes shown are from the same gel. (*G*) In vitro nuclear import assay confirms change in localization of nonexpanded ataxin-3 upon addition of KPNA3 and suggests a role for KPNB1 as partner protein. Nuclear import of ataxin-3 is largely blocked when using the loss-of-function RanQ69L mutant (58). $n = 4$ or 5. (*H*) Visualization of nuclear import assay quantified in *G*. Values are displayed as mean ± SEM for *A*, *C*, and *E*–*G*. $^{*}P < 0.05$; $^{**}P < 0.01$; $^{***}P < 0.005$ [Student's two-sided (*A* and *E*) or one-sided (*F*) *t* test relative to control, with Welche's correction in *G*]. Ataxin-3 was detected with 1H9 antibody in *A* and *F*. Rel., relative.

significance. The filter trap results were confirmed by visual counting (Fig. 1*E*), and overexpressed levels of *KPNA3* and *IPO13* were confirmed by quantitative RT-PCR (qRT-PCR) and Western blot (Fig. 1 *C* and *D*). Furthermore, we fractionated aggregated ataxin-3 to understand which population of aggregates was increased by *KPNA3* overexpression. We were able to see a significant increase in the SDS-insoluble levels (formic acid fraction; Fig. 1*F*), which could be more damaging for the cell, as they are harder to clear than their more soluble counterparts (22). While aggregates served as a surrogate measure for nuclear translocation, we wanted to verify that an increase in aggregation was also correlated to a visual increase in nuclear ataxin-3. To this point, we transfected HEK293 cells with the same constructs of ataxin-3 and transport protein to visualize protein localization by microscopy. Cells that were overexpressing *KPNA3* showed more nuclear ataxin-3 than cells without additional KPNA3 (Fig. 1*B*), while cells overexpressing IPO13 or CRM1 [a protein previously implicated in ataxin-3 shuttling (23)] showed no difference in protein localization. We postulated that KPNA3 must thus be involved in an interaction with ataxin-3 which facilitates its transport. Our analysis using the STRING interaction prediction algorithm suggested that the interaction between the two proteins occurs through Ran (Ras-related nuclear protein) and KPNB1, a known interaction partner of KPNA3 which forms a classic importin alpha/beta Ran dependent complex. Thus, we performed an analysis to see whether altering levels of KPNB1 or Ran would alter the observed nuclear import of ataxin-3 by KPNA3. We did, in fact, see that either a disturbance in KPNB1 or the Ran gradient through the use of a Ran mutant decreased the ability of KPNA3 to import ataxin-3 into the nucleus (Fig. 1 *G* and *H*). The enhancement of nuclear translocation with KPNB1 further suggested that an interaction with KPNA3 could proceed through this trimeric complex (24) (Figs. 1*H* and 6).

**Kap-α3, the *Drosophila* Ortholog of Human KPNA3, Controls the Intracellular Localization of Ataxin-3 in Vivo.** Although cell models serve an important purpose in initial research for polyglutamine diseases, they have a number of limitations. Thus, we complemented our studies using *Drosophila* models that recapitulate many aspects of neurodegenerative diseases (25). SCA3-relevant phenotypes, such as progressive neurodegeneration, behavioral abnormalities, and early death, can all be well observed. We reproduced these features in several *Drosophila* SCA3 models to study the effect of *Kap-α3*, the *Drosophila* ortholog of human *KPNA3* and *KPNA4*, on ataxin-3–induced toxicity (Tables S3 and S4). We used multiple concepts in *Drosophila* analysis by validating our results in different lines across various backgrounds. First, we used a lio-GAL4, UAS-ataxin3-Q70 line (designated SCA3) to drive expression of full-length ataxin-3 in salivary glands (SGs) of developing larvae. SG cells are large and allowed us to visualize the effect of *Kap-α3* overexpression (designated Kap-α3 OE) or RNAi-mediated knockdown (designated Kap-α3 KD) on ataxin-3 localization. To validate our findings, we used three available RNAi lines targeting different parts of the gene that reduced the *Kap-α3* mRNA level to 73% (v36104), 60% (v106249), and 45% (JF02686) compared with control animals (Fig. S1). We crossed the SCA3 lines to either *Kap-α3* or control lines (designated SCA3+Kap-α3 OE/KD and SCA3+Control), extracted SGs from the resulting larvae, and performed immunostaining against ataxin-3. As expected, overexpression of *Kap-α3* (UASp-Kap-α3) increased nuclear localization of expanded ataxin-3, whereas knockdown of this protein increased cytoplasmic localization of ataxin-3, thereby confirming our in vitro results in vivo (Fig. 2*B*). This was independently confirmed on a second full-length ataxin-3 line.

**CRM1 Overexpression in *Drosophila* Shows Potential Benefits in SCA3 While IPO13 Impacts Development.** Similar to our in vitro data, *Emb* (the *Drosophila* ortholog of *CRM1*) overexpression and knockdown and *Cdm* (the *Drosophila* ortholog of *IPO13*) knockdown did not affect localization of ataxin-3, while overexpression of *Cdm* did not produce any viable offspring (likely due to lio-GAL4 expression outside of SGs), suggesting a role for *Cdm*/*IPO13* in embryonic development (Fig. 2 *C* and *D*). Next, we wanted to investigate whether these transport proteins can directly regulate neurodegenerative processes. We used the GMR driver in combination with the GAL4 protein to express ataxin-3 and simultaneously modulate the level of Emb/CRM1, Cdm/IPO13, and Kap-α3/KPNA3 in the *Drosophila* eye. We used well-established SCA3 fly lines with truncated expanded ataxin-3 (MJD.tr-Q78) in different genetic backgrounds to observe the rough eye (26). *Emb*/*CRM1* knockdown in SCA3 flies (SCA3+CRM1 KD) had a severe deleterious effect on the eye morphology, as has been reported (26, 27), while *Emb* overexpression demonstrated no or a moderate rescue in necrosis and morphology (SCA3+CRM1 OE; Fig. 3*C*). These features are in agreement with previously described CRM1 functions, as a knockdown of *CRM1* is known to disturb the Ran gradient and other vital cellular functions (28), while the up-regulation of *CRM1* is thought to stimulate prosurvival pathways (29), which points to its wide-reaching effects throughout the cell. In the *Cdm*/*IPO13 Drosophila* lines, we observed a slight improvement with *Cdm*/*IPO13* overexpressing lines (SCA3+IPO13 OE) and no effect with *Cdm*/*IPO13* knockdown lines (SCA3+IPO13 KD; Fig. 3*D*). No effect on the rough-eye phenotype (REP) was observed when modulating these transport proteins without the expanded ataxin-3 protein present (Fig. 3 *E*–*H*). The next step was to use an inducible neuronal driver (elav-GS) which targets full-length ataxin-3 in a neuron-specific manner to analyze the effect of transport proteins on the longevity of adult flies. *Cdm*/*IPO13* knockdown and overexpression had no effect on prolonged survival and also produced very few offspring (again pointing to a pivotal role in development) (Fig. 2*E*). In contrast, *Emb*/*CRM1* knockdown had detrimental effects on longevity (as expected), while overexpression of *Emb* had the largest rescue of survival in the proteins assayed (Fig. 2*E*). In an analysis of locomotor activity to evaluate the progression of ataxia, *Emb*/*CRM1* knockdown had a severe effect on both the induced and uninduced lines, while its up-regulation was able to slightly rescue the locomotor activity (Fig. 2*F*).

Overall, the *Drosophila* experiments with *Emb* and *Cdm* confirmed previous data on *Emb*/*CRM1* knockdown, giving validity to our further results and showing that *Emb*/*CRM1* overexpression has the potential for positive effects in SCA3 through mechanisms that do not appear to involve ataxin-3 localization. *Cdm*/*IPO13* showed no strong effect on either eye phenotype or longevity, but was concerned with toxicity identified by decrease in offspring when expressed with SG or neuronal drivers.

**Kap-α3 Modulates Neurodegeneration and the Neurological Phenotype Associated with Expanded Ataxin-3 in Vivo.** In the *Drosophila* experiments, Kap-α3/KPNA3 behaved in accordance with the in vitro experiments without significant side effects. In presence of MJD.tr-Q78, *Kap-α3* overexpression with a GMR driver worsened the eye phenotype with collapse of the outer structure, prominent degeneration of the ommatidia, and necrotic lesions seen as black spots. Knockdown of *Kap-α3* moderately alleviated the eye phenotype (Fig. 3*B*). Most importantly, GMR-GAL4–mediated modulation of *Kap-α3* without ataxin-3 expression showed no changes to the eye phenotype, confirming that the observed effects are ataxin-3–specific (Fig. 3*F*). The GMR driver is expressed during development and leads to a strong phenotype which is already observed at emergence. Therefore, to investigate whether later modulation of *Kap-α3* may interfere with the MJD.tr-Q78–induced photoreceptor degeneration during adulthood, we turned to the rhodopsin1-GAL4 driver (rh-GAL4), which is expressed only in the late pupal stage. In young rh1> MJD.tr-Q78 flies (8 d), retinal sections did not exhibit specific defects in ataxin-3–expressing flies or when *Kap-α3* was simultaneously overexpressed or depleted (Fig. 3 *I*–*K*). However, in older flies (20 d), the retinas exhibited striking degenerative phenotypes with disorganized ommatidia and tissue dissociation associated with the appearance of vacuoles. Depletion of *Kap-α3* rescued the degenerative phenotype to a large

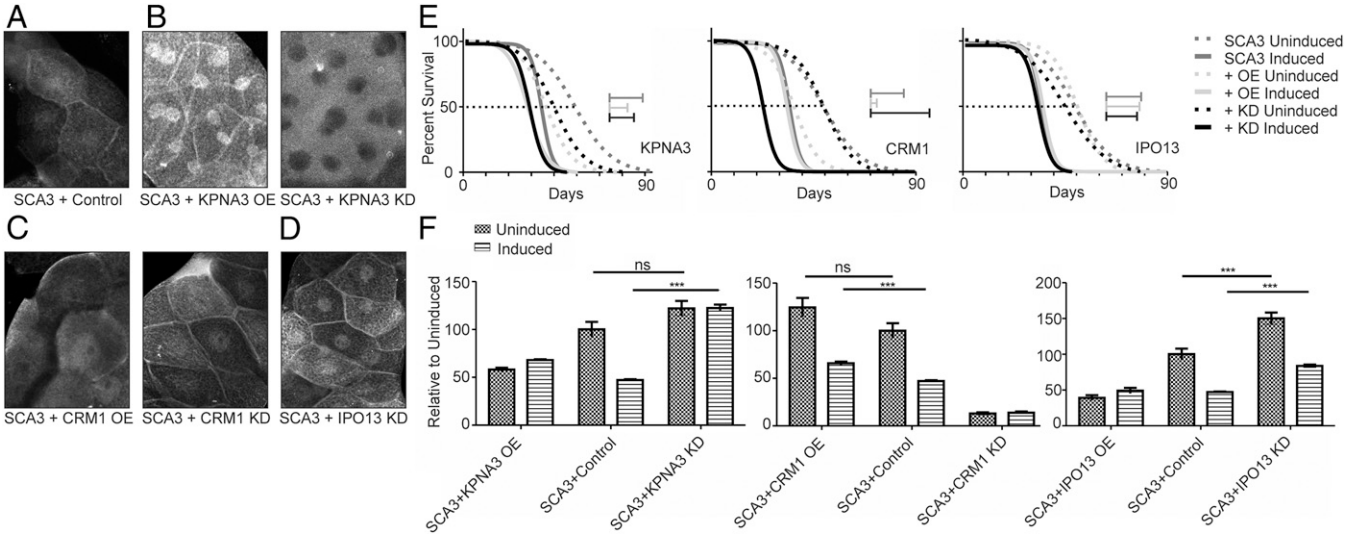


**Fig. 2.** *Kap-α3* controls the intracellular localization of full-length ataxin-3 in *Drosophila* and mitigates the behavioral deficits observed in the SCA3 phenotype. (*A*–*D*) Ataxin-3 immunostaining with 1H9 anti–ataxin-3 antibody in SGs of *Drosophila* larvae expressing full-length ataxin-3 with or without overexpression (OE) or knockdown (KD) of *Kap-α3*/*KPNA3*, *Emb*/*CRM1*, or *Cdm*/*IPO13* genes. (*A*) Control ataxin-3 distribution in SGs. (*B*) Overexpression of *KPNA3* relocates the expanded ataxin-3 protein to the nucleus (*Left*), whereas with *KPNA3* knockdown, ataxin-3 is preferentially cytosolic (*Right*). (*C*) CRM1 modulation does not impact full-length expanded ataxin-3 localization. (*D*) *IPO13* knockdown shows a mild increase in nuclear localization. Overexpression produced no offspring. (*E* and *F*) MLS (*E*) and total activity (*F*) of flies expressing or not in neurons the full-length ataxin-3 with or without modulation of the expression of *Kap-α3*/*KPNA3*, *Emb*/*CRM1*, or *Cdm*/*IPO13* genes. (*E*) *CRM1* knockdown significantly reduced survival of flies, while *CRM1* overexpression had the largest positive effect on survival. *IPO13* had no effect on survival, while *KPNA3* knockdown and overexpression both slightly improved longevity, although not significantly. Differences in longevity are assayed relative to decrease in survival upon induction of ataxin-3. Gray bar demonstrates the decrease in median longevity caused by the induction of ataxin-3 expression. Lighter (overexpression; OE) and darker (knockdown; KD) bars represent the differences with transport proteins. A smaller bar shows a rescue in longevity. Viability was measured on 90–200 flies per genotype. Graphs are shown as nonlinear fit curves of the survival data. (*F*) Total activity of flies. The loss of total activity seen with ataxin-3–induced expression is rescued with *KPNA3* knockdown. Total activity was measured by the amount of light beam breaks produced by movement of one fly per tube in a *Drosophila* Activity Monitor (TriKinetics) over the course of 3 d. Uninduced, $n = 8$; induced $n = 24$; except for *KPNA3* overexpression: uninduced, $n = 16$; induced, $n = 48$. $^{*}P < 0.05$; $^{**}P < 0.01$; $^{***}P < 0.005$; n.s., not significant (one-way ANOVA). Values are displayed as mean ± SEM. RU486 was used in both survival and activity studies to induce the expression of ataxin-3.

extent (Fig. 3 *L*–*N*), while *Kap-α3* overexpression did not significantly aggravate the phenotype. Interestingly, this rescue was also associated with a decrease in ataxin-3 aggregates in retina (Fig. 3*P*), which may result from the change of truncated ataxin-3 localization as observed in SGs (similar to the full-length form) when *Kap-α3* is depleted (Fig. 3*O*). We confirmed that the transcription level of truncated ataxin-3 was not affected by the down-regulation of *Kap-α3* (Fig. S2).

To further evaluate the ability of Kap-α3 modulation to impact the toxicity of mutant ataxin-3, longevity experiments were performed with full-length ataxin-3–expressing flies (Fig. 2*E*). Compared with uninduced flies, the induced elavGS> ataxin3-Q70 flies exhibited a shorter mean lifespan (MLS) as measured by the ratio $R = \mathrm{MLS}^{\mathrm{RU100}}/\mathrm{MLS}^{\mathrm{RU0}} = 0.645$, which indicates the extent of toxicity in this genetic background. Importantly, we observed a higher ratio $R$ in elavGS> ataxin3-Q70 flies depleted in Kap-α3 ($R = \mathrm{MLS}^{\mathrm{RU100}}/\mathrm{MLS}^{\mathrm{RU0}} = 0.709$ and 0.872 for two different lines), compared with flies containing wild-type levels of Kap-α3 ($R = 0.645$). This suggests that the ataxin-3–mediated toxicity is mitigated when Kap-α3 is depleted. In addition, examining the locomotor activity in SCA3 flies as measured by TriKinetics activity monitors, we found that the total locomotor activity was strongly affected by ataxin-3 expression, while it was rescued when Kap-α3 was depleted (Fig. 2*F*).

Overall, in our fly studies, KPNA3 demonstrated the most promising effect, which could be considered more specific than CRM1 and more beneficial than IPO13. We observed that Kap-α3/KPNA3 affected ataxin-3 nucleocytoplasmic transport in flies and that partial knockdown of this transport protein rescued progressive photoreceptor neurodegeneration, aggregation, and total activity deficits. This is in agreement with our cell culture models, where *KPNA3* overexpression was able to increase total aggregation and nuclear localization of ataxin-3.

**Knockout of *KPNA3* Keeps Expanded Ataxin-3 in the Cytoplasm and Prevents Its Aggregation in Mice.** After confirming the importance of its ortholog of KPNA3 for the development of an ataxin-3–induced phenotype in *Drosophila*, we replicated our results in a mouse model. We first obtained *KPNA3*$^{-/-}$ MEF cells and transfected them with expanded GFP-tagged ataxin-3. Compared with wild-type MEF cells, *KPNA3* knockout MEF cells showed a more prominent cytoplasmic distribution of ataxin-3 (Fig. 4*A*). Thus, we generated a SCA3/*KPNA3*$^{-/-}$ mouse model by crossing CamKII/SCA3 77Q mice (designated SCA3) with *KPNA3* knockout mice (designated *KPNA3*$^{-/-}$) (30) to evaluate the effect of the loss of KPNA3 on SCA3 disease progression. CamKII/SCA3 77Q mice were generated by crossing our inducible SCA3 mouse model (31) with the CamKII promoter mouse line (32), resulting in a neuronal expression of ataxin-3 (33). Mice that express both the transgene and have a *KPNA3* knockout were designated as SCA3/*KPNA3*$^{-/-}$ mice. We confirmed the loss of KPNA3 and the presence of the ataxin-3 transgene by Western blot analysis (Fig. 4*B*). We analyzed the localization of KPNA3 in neurons of SCA3 mice and observed no differences with control mice. The next step in this analysis was to test whether the localization and aggregation effects we observed in vitro and in *Drosophila* were reproducible in our rodent models. We killed animals at 12 mo of age and ran whole-brain lysates through filter trap analysis to visualize the total aggregated protein (Fig. 4*C*). We observed that an increase in aggregation in our SCA3 model was rescued in the SCA3/*KPNA3*$^{-/-}$ mouse model (Fig. 4*C*). This was in line with an observed trend in the reduction of ataxin-3 upon the knockout of *KPNA3*, possibly due to enhanced clearance of cytoplasmic ataxin-3 (Fig. 4*B*). We subsequently performed immunohistochemical analysis of ataxin-3 in brains of SCA3/*KPNA3*$^{-/-}$ mice

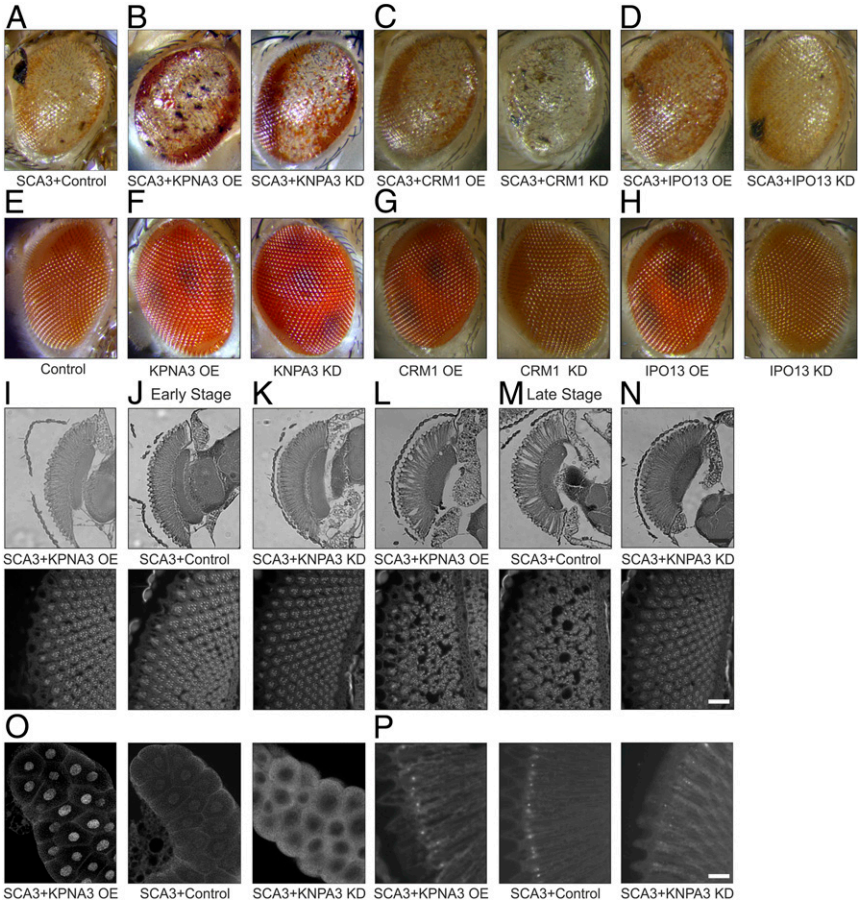


**Fig. 3.** Morphology of *Drosophila* eye is drastically altered by truncated ataxin-3 and subsequently rescued by *Kap-α3/KPNA3* knockdown. (*A–D*) *Drosophila* expressing expanded ataxin-3 show depigmentation, necrotic spots, and disordered bristles (*A*), which is increased by *Kap-α3/KPNA3* overexpression (*B*, *Left*) and improved with knockdown (*B*, *Right*). *Emb/CRM1* (*C*, *Left*) and *Cdm/IPO13* (*D*, *Left*) overexpression improved the phenotype, while knockdown either did not act on the phenotype (IPO13, *D*, *Right*) or worsened it (CRM1, *C*, *Right*). (*E–H*) Control flies without ataxin-3 (*E*) or only with transport proteins (*F–H*) had normal eyes. (*I–N*) Full (*Upper*) and internal (*Lower*) retinal sections. (*I–K*) At early stage (8 d), expanded ataxin-3 expression did not lead to a strong eye phenotype (*J*) which is not impacted by KPNA3 (*I* and *K*). (*L–N*) At late stage (20 d), eyes showed retinal vacuoles and photoreceptor disorganization (*M*). Overexpressing *KPNA3* had no impact (*L*); down-regulation rescued global retinal morphology (*N*) ($n = 12$ flies per genotype). [Scale bars: 50 μm (*Upper*) and 10 μm (*Lower*).] (*O*) Immunostaining with anti-1C2 polyQ antibody in SGs of *Drosophila* larvae expressing truncated ataxin-3. *Kap-α3/KPNA3* overexpression localized ataxin-3 in the nucleus (*O*, *Left*) and down-regulation in the cytoplasm (*O*, *Right*). (*P*) Ataxin-3 immunostaining with anti-HA in 8-d-old retina *Drosophila* expressing expanded ataxin-3 leading to nuclear aggregate formation (*P*, *Center*). *KPNA3* knockdown decreased the amount of aggregates (*P*, *Right*), while overexpressing KPNA3 did not act on it ($n > 7$ per genotype). (Scale bar: 10 μm.)

and in SCA3 animals (Fig. 4*D*). We observed a shift of ataxin-3 staining from the nucleus to the cytoplasm in neurons of SCA3/*KPNA3*$^{-/-}$ compared with SCA3 animals, thus providing further evidence that KPNA3 is directly involved in the pathogenic pathways behind aggregate formation and, likely, neurodegeneration. We further identified that SCA3 animals consume less food than their other littermates, but do not weigh less by 12 mo of age. This could point to a metabolic defect which has yet to be elucidated but is also improved in the *KPNA3* knockout background (Fig. 4 *E* and *F*).

**The Knockout of *KPNA3* Alleviates the Neurological Phenotype Induced by Expanded Ataxin-3 in Vivo.** Since the clinical manifestation of the disease symptoms in SCA3 patients is variable, we explored multiple levels of pathology in our animals to analyze the effect of *KPNA3* knockout. First, we analyzed the overall activity of mice using home-cage analyses. At 11 mo of age, SCA3 mice showed an increase in activity during the dark phase which was almost double that of control animals (Fig. 5 *A* and *B*). This hyperactivity was correlated to a decrease in anxiety as shown by an increase in the exploration of the center of the home cage (Fig. 5 *C* and *D*). *KPNA3* knockout rescued these total activity and anxiety deficits (Fig. 5). We then investigated classical neurological symptoms. SCA3 patients suffer from an impaired gait, including a reduced cadence and a reduced stride (34, 35). As cerebellar ataxia is described as a combination of various movement conditions, such as inability to coordinate movement, abnormal movement patterns, and disturbances in the rhythmicity of movement (36), we analyzed the nuanced nature of these abnormalities in our mice. We observed that SCA3 animals had a slower pace and cadence, mimicking the shuffled, slow gait of patients. This phenotype was largely improved by *KPNA3* knockout (Fig. 5 *F* and *G*). We also observed differences in the base of support and visual distribution of footsteps, but quantification did not reach statistical significance (Fig. 5*E*). To analyze the pattern of movements, we analyzed the phase dispersion of paw steps, which tracks how the paws are placed in relation to each other. Both the front- and hind-paw phase dispersion was decreased in SCA3 animals, suggesting that they placed their other front or hind paw down sooner than expected in a normal gait, probably to support an unsteady, ataxic walk. This phenotype was statistically significantly rescued with *KPNA3* knockout (Fig. 5*H*).

In summary, we demonstrated in cells, *Drosophila*, and mice that KPNA3 is a key player in the pathogenesis in SCA3: Its down-regulation keeps ataxin-3 in the cytoplasm alleviates the toxicity of expanded ataxin-3 and thereby phenotypic features in SCA3 models.

## Discussion

The nuclear localization of expanded ataxin-3 confers a pathogenicity to the expanded protein whereby the protein hyperaggregates and clearance of aggregates is deterred. Altering this localization was previously studied via various pathways such as inhibition of calpains or phosphorylation, but our work targets transport proteins (karyopherins) to explore their role in the pathogenic process (10, 11, 23, 37). We suggest that KPNA3 is a key player in the nuclear localization of ataxin-3 and that altering this localization mitigates the disease process (Fig. 6). After screening a subset of transport proteins in HEK cells, we identified three potential candidates (KPNA3, IPO13, and CRM1) for which the in vivo roles in SCA3 and neurodegenerative diseases in general have not been studied. We believe our findings will provide important insights into these proteins in the context of polyglutamine diseases.

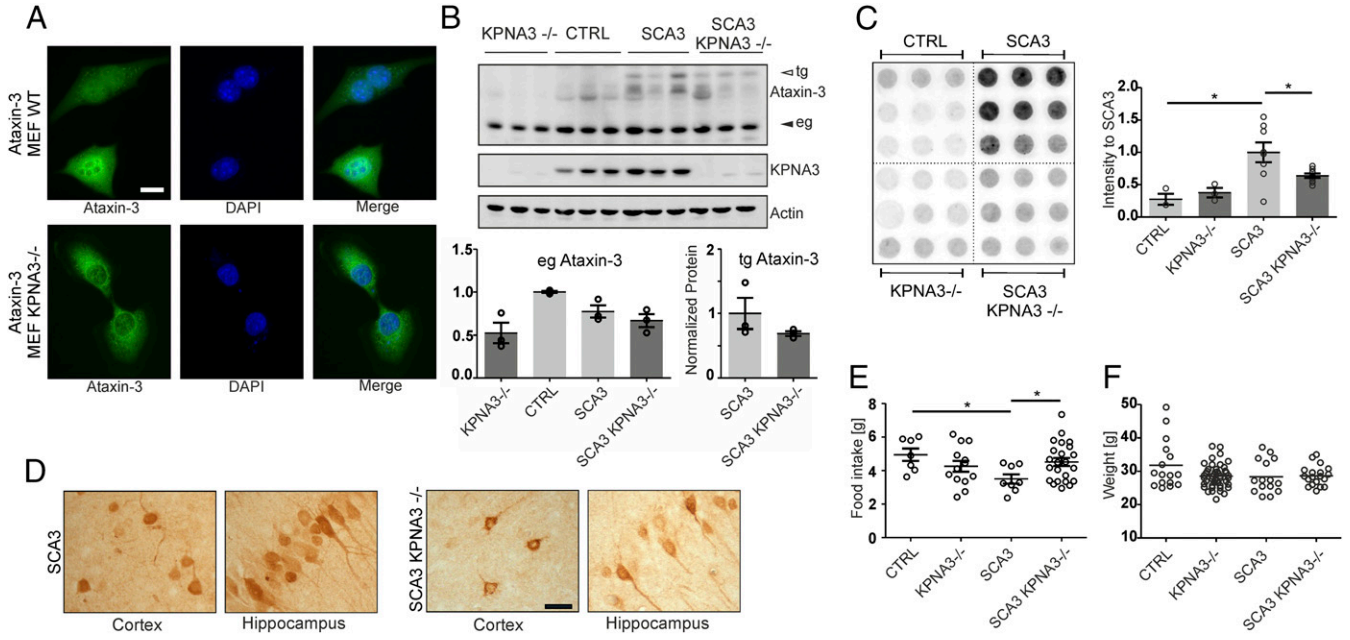


**Fig. 4.** The knockout of *KPNA3* reduces the amount of aggregated protein in brains of SCA3 mice and increases the cytoplasmic distribution of expanded ataxin-3. (*A*) Mouse embryonic fibroblasts (MEFs) from *KPNA3*$^{-/-}$ mice show a strong cytoplasmic distribution of transfected ataxin-3 compared with WT MEFs. (Scale bar: 20 μm.) (*B*) Analysis of 12-mo-old SCA3/*KPNA3*$^{-/-}$ mouse whole-brain lysate showed an expression of transgenic ataxin-3 (tg) in addition to the codetected endogenous ataxin-3 (eg) and a knockout of *KPNA3* with quantification. $n = 3$. (*C*) Aggregated ataxin-3 from a whole-brain lysate of 12-mo-old mice. SCA3/*KPNA3*$^{-/-}$ mice showed a statistically significant reduction compared with SCA3 mice. Heterozygous *KPNA3* knockouts were used as controls. Quantification was done by using LI-COR Image Studio (LI-COR Biosciences). Control (CTRL), $n = 3$; *KPNA3*$^{-/-}$, $n = 3$; *SCA3,* $n = 8$; SCA3/*KPNA3*$^{-/-}$, $n = 8$. Results from three mice from each genotype are shown as a composite of one filter trap, and each row shows three technical replicates from one mouse. Quantification is shown in *C, Right*. (*D*) Change in localization of ataxin-3 was assayed by microscopy. Pyramidal cells in mouse cortex and hippocampal cells show increased cytoplasmic distribution of ataxin-3 in SCA3/*KPNA3*$^{-/-}$ mice compared with SCA3 animals as detected with DAB. (Scale bar: 50 μm.) (*E* and *F*) SCA3 animals did not show a marked decrease in weight compared with wild-type group (*F*), although they consumed 30% less food in 24 h (*E*), which points to metabolic deficits in energy maintenance. Weight: WT, $n = 16$; *KPNA3*$^{-/-}$, $n = 46$; SCA3, $n = 15$; SCA3 *KPNA3*$^{-/-}$, $n = 19$. Mean age: 12 mo. Food consumption: WT, $n = 7$; *KPNA3*$^{-/-}$, $n = 13$; SCA3, $n = 8$; SCA3 *KPNA3*$^{-/-}$, $n = 23$. Mean age: 5 mo. *$P < 0.05$ (Student's *t* test). Values are displayed as mean ± SEM 1H9 ataxin-3 antibody in *C* and *D*.

**Modulating CRM1 Had Reproducible and Promising Effects for SCA3 Pathology.** Of all of the transport proteins screened, CRM1 has garnered the most attention in the field of polyglutamine disease. One reason could be the ability to inhibit CRM1 function with leptomycin B, a promising development in the field of cancer (28). The *Drosophila* ortholog of *CRM1* (*Emb*) was previously shown to be a modifier of ataxin-3 toxicity in two screens (26, 27). We were able to replicate the degeneration in the REP of *Drosophila* with *Emb* knockdown and additionally showed a rescue with *Emb* overexpression. Although we did not see direct aggregation or localization difference with the modification of the protein, this can be explained by the fact that CRM1 serves a more passive function in export, and overexpressing the protein does not increase specificity for ataxin-3 enough to make a difference in the assays we used. Correlating the REP to longevity showed that *Emb* knockdown had negative consequences on lifespan and that overexpression of the protein was able to rescue the relative lifespan in *Drosophila*, which has not been previously demonstrated. It is possible that CRM1 up-regulation will serve as a potential therapeutic in neurodegenerative disease in the future as the true targets of this protein are uncovered.

**Modulating the IPO13 Ortholog Has Severe Consequences for *Drosophila* Viability.** *IPO13* overexpression reduced protein aggregation in our screen, but also showed a multitude of warning signs, including an inability to produce any viable flies overexpressing IPO13 and ataxin-3 in the SGs and whole-body expression. We had a reduced number of offspring in the longevity analysis with this line. This suggests that IPO13 has a detrimental effect on the developmental processes involved in larvae-to-adult progression. IPO13 was shown to be localized in the cytoplasm at early stages of embryonic mouse development and relocates to the nucleus at late stages in neuronal cells. It appears that the effects of IPO13 are differentially regulated during neuronal development. Perhaps IPO13 is responsible for ataxin-3 trafficking during specific stages of brain development, which we were not able to isolate (38). In summary, the pathways of IPO13 regulation have the potential to positively rescue the SCA3 phenotype, but only after more careful consideration of the neuronal timing of expression and an explanation for the decrease in producing viable offspring. It also still needs to be explored whether reproduction and longevity are altered by *IPO13* overexpression in other species than *Drosophila*. It can be suggested that models expressing *IPO13* at higher levels could give insights for future studies as to whether this could be a suitable therapeutic approach.

**KPNA3 Controls the Intracellular Localization and Aggregation of Ataxin-3 in Vitro and in Vivo.** Compared with CRM1 and IPO13, KPNA3 was able to modulate the localization and behavior phenotypes without severe consequences of knockout in the mouse model. Thus, we believed it to be the most viable choice for more targeted investigation. Here, we used aggregation analyses as a starting point and readout to show that *KPNA3* overexpression was able to increase total aggregation in vitro and confirmed in vivo that modifying the level of KPNA3 alters the localization of expanded ataxin-3. A reduction or knockout of *KPNA3* and subsequent localization of ataxin-3 to the cytoplasm may also have downstream consequences such as enhanced clearance and degradation of the protein—a mechanism which requires further clarification, thus defining the underlying cytoplasmic factors. Another interesting point is that we could show, in SGs, a change in ataxin-3 localization with both the truncated and full-length expanded ataxin-3 constructs giving way to three possible

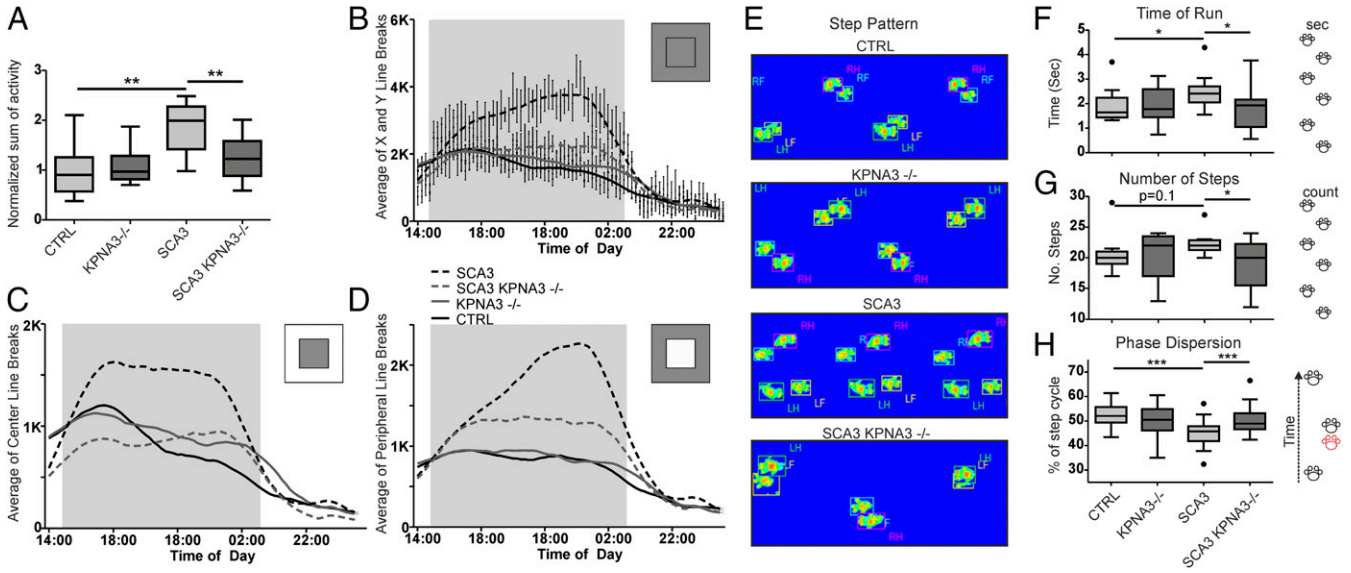


**Fig. 5.** Hyperactivity and reduced anxiety as well as temporal and special gait disturbances of SCA3 mice are improved with *KPNA3* knockout. (*A–D*) Total activity was measured by line breaks in the PhenoMaster Home Cage System (TSE Systems) in the *x* and *y* axis and is binned in 15-min intervals. Data are shown in *B–D*. *A* is a quantification of the total activity during the dark phase represented in *B*. (*A*) Total activity of SCA3 mice ($n = 6$) during the dark/active phase was increased to double of controls (CTRL; $n = 14$). The knockout of *KPNA3* (in SCA3/*KPNA3*$^{-/-}$ mice; $n = 15$) rescued activity to control levels. All values were normalized to the activity of control mice and are represented as mean ± SEM. *KPNA3*$^{-/-}$, n = 13. (*B–D*) Graphs demonstrating the total activity (*B*), center (*C*), and peripheral (*D*) activity over the full 20 h of measurement. Individual points are overlaid with a smoothed curve per GraphPad. SCA3 mice show statistically significant hyperactivity as analyzed by one-way ANOVA ($P < 0.005$) and subsequent Bonferroni's multiple comparison in *B*, while SCA3/*KPNA3*$^{-/-}$ did not differ from control mice (CTRL). The dark phase is shown in gray. Mean age was 11 mo. (*E–H*) Animals were analyzed on the CatWalk gait analysis system (Noldus Information Technology) at 11 mo of age. (*E*) Representative step patterns to demonstrate SCA3-related gait abnormalities. LF, left front paw; LH, left hind paw; RF, right front paw; RH, right hind paw. (*F*) Compared with control mice (CTRL), SCA3 mice showed an increase in total time taken to complete the run of constant length, alleviated upon knockout of KPNA3 (SCA3/*KPNA3*$^{-/-}$). (*G*) SCA3 mice take more steps to complete the run in comparison with control animals. (*H*) SCA3 mice showed paw control and interpaw coordination deficits as measured by phase dispersion, which is resolved by *KPNA3* knockout. CTRL, $n = 12$; *KPNA3*$^{-/-}$, $n = 7$; SCA3, $n = 8$; SCA3/*KPNA3*$^{-/-}$, $n = 11$. Mean age: 11 mo. All values are shown as mean ± SEM. *$P < 0.05$; **$P < 0.01$, ***$P < 0.005$ (Student's *t* test compared with SCA3 animals).

hypotheses: The first one is that the currently identified NLS present in both constructs is sufficient for KPNA3 binding. It is also plausible that there is another unidentified binding site or that the polyglutamine stretch itself serves as a binding partner for KPNA3. While the exact binding mechanism has to be further investigated, the ability of *KPNB1* overexpression to boost nuclear localization of ataxin-3 in vitro suggests that KPNA3 functions as a nuclear importer of ataxin-3, likely in a trimeric complex of KPNA3 and KPNB1 with ataxin-3. We further expanded our analysis by studying the *Drosophila* eye, a structure well suited to investigate neuronal degeneration. In this model, we observed that overexpression of the *Drosophila* homolog of *KPNA3* increased structure breakdown, the amount of necrosis, and bristle disorganization, which fits to the increase in nuclear ataxin-3 upon overexpression. *KPNA3* knockdown, on the other hand, was able to rescue the REP, photoreceptor degeneration, and nuclear aggregation of ataxin-3. This connection between cellular localization and neuronal function suggested that altering KPNA3 may be an interesting target to modulate disease progression of SCA3. Our hypothesis is also supported by recent studies of ALS which show that KPNA3 is able to increase TDP-43 nuclear localization and studies in SCA6 indicating that knockdown of *Kap-α3* decreased nuclear protein and improved retinal degeneration in flies (39, 40).

**Knockout of *KPNA3* Rescues the Behavioral Phenotype of *Drosophila* and Mouse Models of SCA3.** In a previous study, we demonstrated the critical importance of the nuclear localization of expanded ataxin-3 for the manifestation of symptoms in SCA3 (10). We now show that KPNA3 is the key transport protein to shuffle expanded ataxin-3 into the nucleus and to link it to neuronal dysfunction and death. Thus, we hypothesized that downregulation of *KPNA3* may be an interesting target to rescue behavioral abnormalities caused by polyQ expansion of ataxin-3 in in vivo models. As changes in total activity are well known in animal models of ataxin-3 (41), we used a *Drosophila* activity assay to analyze the effect of modulating *Kap-α3*. In our inducible expression model, SCA3 flies showed a decrease in total activity compared with their uninduced control counterparts. This hypoactivity was rescued to control levels with a knockdown of *Kap-α3*, suggesting that its down-regulation is also able to rescue deficits related to the progression of SCA3. To confirm these data in a rodent model, we analyzed SCA3/*KPNA3*$^{-/-}$ mice, studied their total activity, and compared the readout to their SCA3 and CTRL counterparts. It has been reported that SCA3 mouse models eventually develop hypoactivity as seen in *Drosophila*, but a phase of hyperactivity can be a predecessor to this hypoactive stage (41). Hyperactivity as a sign of neuronal dysfunction has been observed in models for SCA3 (10, 31, 42) as well as in HD (43) and in Parkinson's disease (44). Our mice did, in fact, show a hyperactive phenotype characterized by increased total activity during the dark/active phase. This phenotype progressed throughout the lifespan of the animals and was rescued in the SCA3/*KPNA3*$^{-/-}$ mice. Consistent with our *Drosophila* data, the total activity of our SCA3 mice was brought back to control levels by knocking out *KPNA3*. In the same home-cage analysis, we were also able to assay the anxiety phenotype. The degeneration of the cerebellum and its afferent and efferent regions causes a variety of nonmotor behavior concerns for patients, with disturbance of sleep, depression, and anxiety being the most predominant (45, 46). Animal models are able to mimic these disturbances in anxiety, which present themselves as a decrease in open-space avoidance (10, 31, 42, 47). In our SCA3 animals, this decrease in anxiety was rescued by the knockout of *KPNA3*. This suggests that KPNA3 has an effect on psychiatric symptoms of SCA3 as well as behavioral symptoms such as total activity. This is interesting in relation to the current research which puts KPNA3 at the center of multiple psychiatric disorders.

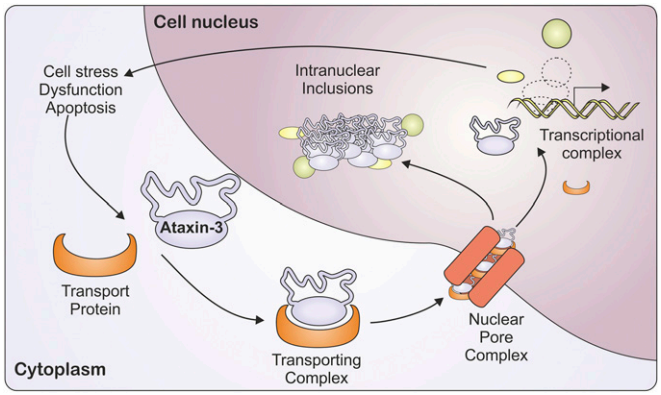


**Fig. 6.** How translocation of the ataxin-3 protein mitigates disease progression of SCA3. The degeneration of neurons runs in a vicious circle where cellular stress both causes more translocation of ataxin-3 into the nucleus and the translocation itself results in more cellular stress. (*i*) Cellular signals cause ataxin-3 to be recruited into the nucleus with the help of KPNA3. (*ii*) Ataxin-3 attempts to serve its function as a transcriptional regulator in the nucleus. (*iii*) In the case of SCA3, expanded ataxin-3 is not able to properly mitigate this process and is also recruited into various aggregate intermediates and large aggregates which capture and trap other proteins. (*iv*) The havoc caused by expanded ataxin-3 being retained in the nucleus causes more cellular stress, which signals for more ataxin-3 to be recruited into the nucleus, causing more damage. (*v*) By targeting nuclear transport, i.e., KPNA3, this aspect of nuclear degeneration could be halted and the neurons rescued.

*KPNA3* single-nucleotide polymorphisms were found to be significantly associated with schizophrenia, opiate dependence and alcohol dependence at the genotype level and with major depressive disorder at the allele level (48). Thus, we conclude that the in vitro findings which show KPNA3's effect on aggregation and localization translate to a rescue of behavior and psychiatric phenotypes in our *Drosophila* and mouse models of SCA3. These data are significant because they add to the body of knowledge which suggests that localization of the ataxin-3 protein is necessary for disease manifestation and that modulating this localization through transport proteins is a way to control the development of these symptoms.

***KPNA3* Knockout Is Able to Rescue Gait Abnormalities in a Mouse Model of SCA3.** While we were able to see differences in total activity and anxiety with the home-cage analysis, we wanted to know if the benefits of *KPNA3* knockout also extend to the gait phenotype observed in patients and animal models. Gait disturbances are some of the strongest features of SCA3, and the initial description of cerebellar ataxia included difficulty with coordinating movement, issues in muscle tone, and abnormal movement patterns (36). These features can be measured in mouse models and present a way to further analyze the effect of *KPNA3* knockout on SCA3 progression. For this, we employed the CatWalk gait analysis system, which has been used and validated for the analysis of nerve injury but also of neurodegenerative diseases (49). We were able to demonstrate that SCA3 mice took more time to complete the CatWalk compared with CTRL and SCA3/*KPNA3*$^{-/-}$ animals, which correlates to the slower, more shuffled phenotype observed in SCA3 patients. Patients also show a reduced cadence, which is a measure of the number of steps taken in a specific time (34); this was also well-mirrored by our models. The knockout of *KPNA3* in SCA3 mice was able to bring these parameters back to control levels. These measures are important, as they point to specific features of ataxic gait which are directly improved and impacted by *KPNA3* knockout. More recently, joint coordination patterns have been used as balance-independent measurements of ataxia-induced limb coordination impairment (50). Ataxic patients spend more time with feet on the ground, have irregular foot placement, and are unable to keep up a constant walking pattern over time (31, 51). SCA3 animals also showed an inability to maintain this normal walking pattern as measured by phase dispersion (the timing of paw placement in relation to a full stride). SCA3 mice preemptively placed their second paw for either support or lack of coordination, which mirrors both joint coordination and walking pattern issues. It is important to note that these results suggest that the ataxic gait observed in patients and in the SCA3 mouse model is influenced by both balance-related impairments and limb control and intralimb coordination. The crude and more nuanced features together paint a fuller picture of the walking disturbances which can be tracked during disease progression and in animal models. Our data add significant knowledge to the field. Not only have we performed a thorough analysis of the gait in SCA3 animals, but we have also been able to demonstrate that these features can be either fully or partially improved with *KPNA3* knockout.

## Conclusion

Overall, we believe this work opens promising insight into the pathogenesis of SCA3. We have demonstrated that altering transport proteins has an effect on both pathogenic mechanisms (e.g., the intracellular localization and the formation of aggregates) and key features of disease manifestation such as anxiety, total activity, and gait. The downstream mechanisms, possibly involving ataxin-3 clearance and degradation, are still to be investigated, and the correlation of KPNA3 with psychiatric disorders warrants further exploration into the interplay between KPNA3 levels and expansion of ataxin-3 within the patient population. We suggest that a better appreciation of the overall cellular mechanism can enhance our understanding of all polyglutamine diseases as well as aid in the development of novel targets for therapy.

## Materials and Methods

**Cell Culture Analysis.** HEK 293-T, SK-N-AS, and MEF cells were grown at 37 °C and 5% $CO_2$ in supplemented Dulbecco's modified Eagle medium (Invitrogen). For stable transfection, HEK 293-T cells were transfected with GFP-tagged constructs and FACS-sorted for highly expressing cells. Expression constructs were obtained from Origene (TrueClones; OriGene Technologies).

**Aggregate Analysis and Fractionation.** Filter trap analysis were performed as described (52). Cells were collected 96 h posttransfection, measured by Bradford assay (Bio-Rad Laboratories), and run on a cellulose acetate membrane (Carl Roth) with the filter trap apparatus (SRC 96 D Minifold-1 Dot Blotter; Schleicher & Schuell). Aggregate fractionation was performed as described (53). HEK 293-T cells were transiently transfected with GFP ataxin-3 and transport protein constructs and incubated for 72 h. After separation, proteins were transferred to a nitrocellulose membrane (Optitran and Protran; Millipore).

**In Vitro Nuclear Import Assay.** U2OS cells were digitonin-permeabilized and incubated with IP buffer plus (IP buffer, pH 7.5, 10 mg/mL BSA, and 2 mM DTT). The import reaction was started by the addition of import mix containing Ran-GDP, fluorescein-labeled ataxin-3, ATP regeneration system (ATP, GTP, creatine phosphate, and creatine kinase), KPNA3, importinß/KPNB1, RanGAP, RanBP1, and EGTA in IP buffer, pH 7.5. The samples were fixed and analyzed by fluorescence microscopy. DAPI fluorescence was used for single-cell discrimination.

**Western Blot Analysis.** Filter trap and Western blot membranes were essentially detected as described (21). Membranes was detected by using an Odyssey Fc Imager (LI-COR Biosciences) and quantified by using the Image Studio Software (LI-COR).

**Immunofluorescence and Immunohistochemical Stainings.** Cells were fixed with 4% PFA and then incubated with primary and secondary antibody. Immunohistochemical stainings were performed as described (54). Sections were stained by using the biotin-conjugated secondary antibody, detected by using the VECTASTAIN Elite ABC Kit (Vector Laboratories) and 3,3′-diaminobenzidine (DAB; Sigma). Fluorescence and DAB staining was visualized with an Axioplan 2 imaging microscope (Carl Zeiss Microimaging).

***Drosophila* Strains and Housing.** The GMR-GAL4 (FlyBaseID: FBti0002994; Tables S3 and S4), UASp-Kap-alpha3 (FlyBaseID: FBti0101875), Kap-alpha3 [TRiP.JF02686] (FlyBaseID: FBti0128794), and UAS-MJD.tr-Q78 (FlyBaseID: FBti0040564) strains were obtained from the Bloomington Stock Center (Indiana University). The lio-GAL4 (FlyBaseID: FBti0115618) strain was provided by J. M. Dura, Institute of Human Genetics, Montpellier, France. The UAS-ataxin-3-70Q (55) and the da-GS (56) have been described. The sgs{v21206} line is used as a RNAi negative control (since it targets a protein absent in adult flies). This line, the Kap-alpha3 {v36104}, and {v106249} lines were obtained from the Vienna *Drosophila* Resource Center. The elav-GS line was derived by remobilization of the elav-GS-301.2 line (57) and provided a strong neuronal induction.

Fly stocks were maintained on a standard cornmeal–agar–yeast–sugar-based diet at 18 °C. Standard cross-breeding and other experiments with larvae and adult *Drosophila* were conducted at 26 °C on the same diet. Progeny was collected from the day of hatching and sorted by gender and appropriate phenotypic markers. For induction of UAS transgene expression, flies were treated with 100 μg/mL RU486 (in ethanol); uninduced flies were treated with ethanol only.

***Drosophila* SG Expression of Ataxin-3.** SGs from third-instar larvae were dissected, fixed in 4% PFA, permeabilized with 0.1% Triton X in PBS, and blocked with 2% BSA in PBS. To detect ataxin-3, tissues were incubated overnight in 1H9 antibody (1:1,000; Chemicon, Merck Millipore) or anti-HA antibody (1:500; Millipore) at 4 °C. To detect primary antibodies, Alexa Fluor 594 anti-mouse or Alexa Fluor 546 anti-rabbit secondary antibodies (diluted 1:500) were used. Imaging was done with the Zeiss LSM700 confocal microscope. Genotypes in Fig. 2 *A–D* are lio-GAL4, ataxin3-Q70/sgs1{v21206} (SCA3+Control); lio-GAL4, ataxin3-Q70/UASp-Kap-alpha3 (SCA3+KPNA3 OE); lio-GAL4, ataxin3-Q70/Kap-alpha3 [TRiP. JF02686] (SCA3+KPNA3 KD); lio-GAL4, ataxin3-Q70/Emb [EY08770] (SCA3+CRM1 OE); lio-GAL4, ataxin3-Q70/Emb [TRIP.JF01311] (SCA3+CRM1 KD); lio-GAL4, ataxin3-Q70/Cdm [TRIP.JF01428] (SCA3+IPO13 KD). Genotypes in Fig. 3*O* are GAL1118, ataxin3-Q78/sgs1{v21206} (SCA3+Control); GAL1118, ataxin3-Q78/Kap-alpha3 [TRiP.JF02686] (SCA3+KPNA3 KD); GAL1118, ataxin3-Q78/UASp-Kap-alpha3 (SCA3+KPNA3OE).

***Drosophila* REP Modification.** For analysis, flies were grown at 25 °C. Male flies were collected 1 d posthatching and imaged on a Leica M205FA microscope. Genotypes in Fig. 3 *A–D* are GMR-GAL4, MJDtr-78Q/sgs1{v21206} (SCA3+Control); GMR-GAL4, MJDtr-78Q/UASp-Kap-alpha3 (SCA3+KPNA3 OE); GMR-GAL4, MJDtr-78Q/Kap-alpha3 [TRiP.JF02686] (SCA3+KPNA3KD); GMR-GAL4, MJDtr-78Q/Emb [EY08770] (SCA3+CRM1 OE); GMR-GAL4, MJDtr-78Q/Emb [TRIP.JF01311] (SCA3+CRM1 KD); GMR-GAL4, MJDtr-78Q/Cdm GS1766 (SCA3+IPO13 OE); GMR-GAL4, MJDtr-78Q/Cdm [TRIP. JF01428] (SCA3+IPO13 KD). Genotypes in Fig. 3 *E–H* are GMR-GAL4/sgs1 {v21206} (SCA3+Control); GMR-GAL4/UASp-Kap-alpha3 (SCA3+KPNA3 OE); GMR-GAL4/Kap-alpha3 [TRiP.JF02686] (SCA3+KPNA3 KD); GMR-GAL4/Emb [EY08770] (SCA3+CRM1 OE); GMR-GAL4/Emb [TRIP.JF01311] (SCA3+CRM1 KD); GMR-GAL4/Cdm GS1766 (SCA3+IPO13 OE); GMR-GAL4/cdm [TRIP. JF01428] (SCA3+IPO13 KD). Genotypes in Fig. 3 *I–N* and *P* are rh1-GAL4, MJDtr-78Q/sgs1{v21206} (SCA3+Control); rh1-GAL4, MJDtr-78Q/UASp-Kap-alpha3 (SCA3+KPNA3 OE); rh1-GAL4, MJDtr-78Q/Kap-alpha3 [TRiP.JF02686] (SCA3+KPNA3 KD); rh1-GAL4, MJDtr-78Q/Emb [EY08770] (SCA3+CRM1 OE); rh1-GAL4, MJDtr-78Q/Emb [TRIP. JF01311] (SCA3+CRM1 KD); rh1-GAL4, MJDtr-78Q/Cdm GS1766 (SCA3+IPO13 OE); rh1-GAL4, MJDtr-78Q/Cdm [TRIP.JF01428] (SCA3+IPO13 KD).

***Drosophila* Retina Morphology.** Eight- or 20-d-old *Drosophila* heads were paraffin-embedded, and frontal retinal sections (5 μm) were prepared. For global retinal morphology, sections were stained with hematoxylin and eosin and imaged on a Leica DM2000 LED microscope. For aggregates visualization, sections were immune-labeled with the rabbit anti-HA antibody (1:200; Millipore) and the Alexa Fluor 546 anti-rabbit secondary antibody (1:200; Life Technologies). Images were acquired by using a Leica TCS SP5 confocal microscope.

***Drosophila* qRT-PCR.** For validation of *Kap-α3* down-regulation by RNAi, RNA was extracted with TRIzol from 10 flies. After reverse transcription using SuperScript III (Invitrogen), flyrnai verified primers (www.flyrnai.org/flyprimerbank) were used. For Fig. S1, genotypes mentioned (Table S4) were crossed with the da-GS driver. Similar procedures were used with truncated ataxin-3 to evaluate the level of ataxin-3 transcription in elavGS;MJDtr-78Q in the absence or presence of *Kap-α3* RNAi transgenes.

***Drosophila* Activity Analysis.** Spontaneous activity of 22-d-old virgin female flies was measured over three consecutive days by using a *Drosophila* Activity Monitor (TriKinetics). Data were acquired with the DamSystem303 software, and Microsoft Excel was used to analyze total activity over the 3 d. Genotypes in Fig. 2*F* are elav-GS, ataxin3-Q70/sgs1{v21206} (SCA3+Control); elav-GS, ataxin3-Q70/UASp-Kap-alpha3 (SCA3+KPNA3 OE); elav-GS, ataxin3-Q70/Kap-alpha3 [TRiP.JF02686] (SCA3+KPNA3 KD); elav-GS, ataxin3-Q70/Emb [EY08770] (SCA3+CRM1 OE); elav-GS, ataxin3-Q70/Emb [TRIP.JF01311] (SCA3+CRM1 KD); elav-GS, ataxin3-Q70/Cdm GS1766 (SCA3+IPO13 OE); elav-GS, ataxin3-Q70/Cdm [TRIP.JF01428] (SCA3+IPO13 KD).

***Drosophila* Longevity Assay.** Male flies were used except in experiments with the Kap-alpha3{v36104}line where the transgene of interest is on the X chromosome. Flies were raised and selected at 25 °C and grouped into vials containing 30 flies maximum. Flies were transferred to fresh food every 2 d, and death events were counted at this point. When all flies were deceased, calculations were made to extract mean and median (T50) lifespan with Microsoft Excel.

**Mouse Housing and Experiments.** Mice were housed specific pathogen-free in type II long cages on lignocel aspen bedding in groups up to five animals per cage and kept on a 12-h light–dark cycle with a 50–55% relative air humidity. Mice had ad libitum access to food and water. All research and animal care procedures were approved by the district government and performed according to international guidelines for the use of laboratory animals in the Forschungsverfügungsgebäude (FORS) animal facility in Tuebingen, Germany. Animal welfare was routinely monitored by the caretakers of the animal facility and the veterinary service of the University of Tuebingen.

**Mouse Genotyping.** Transgenic animals were identified by using DNA extracted from ear biopsy (Roche High Pure PCR Template Preparation Kit; Roche) as described in ref. 6 (Table S6).

**Preparation of Mouse Samples.** Mice were euthanized by using $CO_2$ and transcardially perfused with PBS. Brain was excised from the cranium, and brain hemispheres were separated sagittally. Hemispheres were flash-frozen in liquid nitrogen and stored at −80 °C.

**Mouse Behavior Testing.** Animals were tested in increments of 3 mo until 12 mo of age, and a break of at least 48 h was applied between different tests. The experimenter was blinded for the genetic status of the mice during the behavioral tests, and the order of mice was independent of their genetic status. Control mice were represented by heterozygous *KPNA3*$^{+/-}$ mice and single transgenic SCA3 mice. During behavior testing, mouse weight was monitored. No significant difference in weight was observed. Spontaneous activity was measured in a home-cage environment by using an automated tracking system (LabMaster; TSE Systems). Mice were recorded for 22 h, which started before the onset of the dark phase. To measure gait abnormalities and footprint disruptions, the CatWalk gait analysis system was used (Noldus). Mice were put on the CatWalk system and allowed to freely cross the runway without interruption. Three runs were gathered with a speed variation <50%.

**Statistical Analysis.** Data are presented as mean ± SEM. Statistical significance was calculated by using GraphPad Prism (GraphPad Software). Student's two- and one-sided *t* tests and two-way ANOVA were used as appropriate. A *P* value of <0.05 was treated as statistically significant. CatWalk, LabMaster Homecage, and TriKinetics parameters were reanalyzed and analyzed with Windows Excel and GraphPad Prism.

**ACKNOWLEDGMENTS.** We thank Gemma Arlandis and Raheleh Heidari for their technical help, Jeannette Huebener-Schmid for her support, Maciej Figiel for graphics, and Nicolas Casadei for statistical support. The work leading to this invention was supported by European Commission Seventh Framework Programme FP7/2010 under Grant 264508 (TreatPolyQ) and the Federal Ministry of Education and Research (PPPT-MJD Grant 01GM1309B) under the umbrella of E-Rare-2 [ERA (European Research Area)-Net for research programmes on rare diseases].

1. Kawaguchi Y, et al. (1994) CAG expansions in a novel gene for Machado-Joseph disease at chromosome 14q32.1. *Nat Genet* 8:221–228.
2. Saute JAM, Jardim LB (2015) Machado Joseph disease: Clinical and genetic aspects, and current treatment. *Expert Opin Orphan Drugs* 3:517–535.
3. Weber JJ, Sowa AS, Binder T, Hübener J (2014) From pathways to targets: Understanding the mechanisms behind polyglutamine disease. *BioMed Res Int* 2014:701758.
4. Schöls L, et al. (1997) Autosomal dominant cerebellar ataxia: Phenotypic differences in genetically defined subtypes? *Ann Neurol* 42:924–932.

5. Cunha-Santos J, et al. (2016) Caloric restriction blocks neuropathology and motor deficits in Machado-Joseph disease mouse models through SIRT1 pathway. *Nat Commun* 7:11445.
6. Schmidt J, et al. (2016) In vivo assessment of riluzole as a potential therapeutic drug for spinocerebellar ataxia type 3. *J Neurochem* 138:150–162.
7. Teixeira-Castro A, et al. (2015) Serotonergic signalling suppresses ataxin 3 aggregation and neurotoxicity in animal models of Machado-Joseph disease. *Brain* 138: 3221–3237.
8. Peters MF, et al. (1999) Nuclear targeting of mutant Huntingtin increases toxicity. *Mol Cell Neurosci* 14:121–128.
9. Nucifora FC, Jr, et al. (2003) Nuclear localization of a non-caspase truncation product of atrophin-1, with an expanded polyglutamine repeat, increases cellular toxicity. *J Biol Chem* 278:13047–13055.
10. Bichelmeier U, et al. (2007) Nuclear localization of ataxin-3 is required for the manifestation of symptoms in SCA3: In vivo evidence. *J Neurosci* 27:7418–7428.
11. Antony PMA, et al. (2009) Identification and functional dissection of localization signals within ataxin-3. *Neurobiol Dis* 36:280–292.
12. Görlich D, Kutay U (1999) Transport between the cell nucleus and the cytoplasm. *Annu Rev Cell Dev Biol* 15:607–660.
13. Kodiha M, Chu A, Matusiewicz N, Stochaj U (2004) Multiple mechanisms promote the inhibition of classical nuclear import upon exposure to severe oxidative stress. *Cell Death Differ* 11:862–874.
14. Fagerlund R, Kinnunen L, Köhler M, Julkunen I, Melén K (2005) NF-kappaB is transported into the nucleus by importin alpha3 and importin alpha4. *J Biol Chem* 280: 15942–15951.
15. Pearson AG, Curtis MA, Waldvogel HJ, Faull RLM, Dragunow M (2005) Activating transcription factor 2 expression in the adult human brain: Association with both neurodegeneration and neurogenesis. *Neuroscience* 133:437–451.
16. Lai K-O, Zhao Y, Ch'ng TH, Martin KC (2008) Importin-mediated retrograde transport of CREB2 from distal processes to the nucleus in neurons. *Proc Natl Acad Sci USA* 105: 17175–17180.
17. Nguyen MM, Harmon RM, Wang Z (2014) Characterization of karyopherins in androgen receptor intracellular trafficking in the yeast model. *Int J Clin Exp Pathol* 7: 2768–2779.
18. Maiuri T, Woloshansky T, Xia J, Truant R (2013) The huntingtin N17 domain is a multifunctional CRM1 and Ran-dependent nuclear and cilial export signal. *Hum Mol Genet* 22:1383–1394.
19. Zheng Z, Li A, Holmes BB, Marasa JC, Diamond MI (2013) An N-terminal nuclear export signal regulates trafficking and aggregation of Huntingtin (Htt) protein exon 1. *J Biol Chem* 288:6063–6071.
20. Paulson HL, et al. (1997) Intranuclear inclusions of expanded polyglutamine protein in spinocerebellar ataxia type 3. *Neuron* 19:333–344.
21. Schmidt T, et al. (1998) An isoform of ataxin-3 accumulates in the nucleus of neuronal cells in affected brain regions of SCA3 patients. *Brain Pathol* 8:669–679.
22. Wong ESP, et al. (2008) Autophagy-mediated clearance of aggresomes is not a universal phenomenon. *Hum Mol Genet* 17:2570–2582.
23. Chan WM, et al. (2011) Expanded polyglutamine domain possesses nuclear export activity which modulates subcellular localization and toxicity of polyQ disease protein via exportin-1. *Hum Mol Genet* 20:1738–1750.
24. Lott K, Cingolani G (2011) The importin β binding domain as a master regulator of nucleocytoplasmic transport. *Biochim Biophys Acta* 1813:1578–1592.
25. Bilen J, Bonini NM (2005) *Drosophila* as a model for human neurodegenerative disease. *Annu Rev Genet* 39:153–171.
26. Bilen J, Bonini NM (2007) Genome-wide screen for modifiers of ataxin-3 neurodegeneration in *Drosophila*. *PLoS Genet* 3:1950–1964.
27. Vossfeldt H, et al. (2012) Large-scale screen for modifiers of ataxin-3-derived polyglutamine-induced toxicity in *Drosophila*. *PLoS One* 7:e47452.
28. Nguyen KT, Holloway MP, Altura RA (2012) The CRM1 nuclear export protein in normal development and disease. *Int J Biochem Mol Biol* 3:137–151.
29. Li A, et al. (2013) Upregulation of CRM1 relates to neuronal apoptosis after traumatic brain injury in adult rats. *J Mol Neurosci* 51:208–218.
30. Rother F, et al. (2011) Importin α7 is essential for zygotic genome activation and early mouse development. *PLoS One* 6:e18310.
31. Boy J, et al. (2009) Reversibility of symptoms in a conditional mouse model of spinocerebellar ataxia type 3. *Hum Mol Genet* 18:4282–4295.
32. Mayford M, et al. (1996) Control of memory formation through regulated expression of a CaMKII transgene. *Science* 274:1678–1683.
33. Odeh F, et al. (2011) Atlas of transgenic Tet-Off Ca2+/calmodulin-dependent protein kinase II and prion protein promoter activity in the mouse brain. *Neuroimage* 54: 2603–2611.
34. Ebersbach G, et al. (1999) Comparative analysis of gait in Parkinson's disease, cerebellar ataxia and subcortical arteriosclerotic encephalopathy. *Brain* 122:1349–1355.
35. Palliyath S, Hallett M, Thomas SL, Lebiedowska MK (1998) Gait in patients with cerebellar ataxia. *Mov Disord* 13:958–964.
36. Holmes G (1939) The cerebellum of man. *Brain* 62:1–30.
37. Mueller T, et al. (2009) CK2-dependent phosphorylation determines cellular localization and stability of ataxin-3. *Hum Mol Genet* 18:3334–3343.
38. You P, Peng Z, Wang Y, Tao T (2013) Expression and subcellular distribution of imp13 are regulated in brain development. *In Vitro Cell Dev Biol Anim* 49:346–353.
39. Tsou W-L, et al. (2015) DnaJ-1 and karyopherin α3 suppress degeneration in a new Drosophila model of spinocerebellar ataxia type 6. *Hum Mol Genet* 24:4385–4396.
40. Khosravi B, et al. (2017) Cytoplasmic poly-GA aggregates impair nuclear import of TDP-43 in C9orf72 ALS/FTLD. *Hum Mol Genet* 26:790–800.
41. Colomer Gould VF (2012) Mouse models of spinocerebellar ataxia type 3 (Machado-Joseph disease). *Neurotherapeutics* 9:285–296.
42. Boy J, et al. (2010) A transgenic mouse model of spinocerebellar ataxia type 3 resembling late disease onset and gender-specific instability of CAG repeats. *Neurobiol Dis* 37:284–293.
43. Zala D, et al. (2004) Long-term lentiviral-mediated expression of ciliary neurotrophic factor in the striatum of Huntington's disease transgenic mice. *Exp Neurol* 185:26–35.
44. Graham DR, Sidhu A (2010) Mice expressing the A53T mutant form of human alpha-synuclein exhibit hyperactivity and reduced anxiety-like behavior. *J Neurosci Res* 88: 1777–1783.
45. McMurtray AM, Clark DG, Flood MK, Perlman S, Mendez MF (2006) Depressive and memory symptoms as presenting features of spinocerebellar ataxia. *J Neuropsychiatry Clin Neurosci* 18:420–422.
46. Almeida-Silva UC, Hallak JEC, Júnior WM, Osório FdeL (2013) Association between spinocerebellar ataxias caused by glutamine expansion and psychiatric and neuropsychological signals–A literature review. *Am J Neurodegener Dis* 2:57–69.
47. Bailey KR, Crawley JN (2009) Anxiety-related behaviors in mice. *Methods of Behavior Analysis in Neuroscience* (CRC, Boca Raton, FL).
48. Morris CP, et al. (2012) KPNA3 variation is associated with schizophrenia, major depression, opiate dependence and alcohol dependence. *Dis Markers* 33:163–170.
49. Kyriakou EI, van de Kieft J, Nguyen HP, van der Harst JE (2014) Defining parameters in automated quantitative gait analysis for evaluation of progressive neurodegeneration in animal models of ataxia and motor coordination impairments. *Proc Meas Behav* 2014:29–31.
50. Ilg W, Golla H, Thier P, Giese MA (2007) Specific influences of cerebellar dysfunctions on gait. *Brain* 130:786–798.
51. Serrao M, et al. (2012) Gait pattern in inherited cerebellar ataxias. *Cerebellum* 11: 194–211.
52. Wanker EE, et al. (1999) Membrane filter assay for detection of amyloid-like polyglutamine-containing protein aggregates. *Methods Enzymol* 309:375–386.
53. Koch P, et al. (2011) Excitation-induced ataxin-3 aggregation in neurons from patients with Machado-Joseph disease. *Nature* 480:543–546.
54. Schmidt T, et al. (2002) Protein surveillance machinery in brains with spinocerebellar ataxia type 3: Redistribution and differential recruitment of 26S proteasome subunits and chaperones to neuronal intranuclear inclusions. *Ann Neurol* 51:302–310.
55. Reinhardt A, et al. (2012) Lack of miRNA misregulation at early pathological stages in Drosophila neurodegenerative disease models. *Front Genet* 3:226.
56. Tricoire H, et al. (2009) The steroid hormone receptor EcR finely modulates Drosophila lifespan during adulthood in a sex-specific manner. *Mech Ageing Dev* 130:547–552.
57. Osterwalder T, Yoon KS, White BH, Keshishian H (2001) A conditional tissue-specific transgene expression system using inducible GAL4. *Proc Natl Acad Sci USA* 98: 12596–12601.
58. Palacios I, Weis K, Klebe C, Mattaj IW, Dingwall C (1996) RAN/TC4 mutants identify a common requirement for snRNP and protein import into the nucleus. *J Cell Biol* 133: 485–494.